2007

Reactivity and Sintering Kinetics of Au/ TiO2(110) Model Catalysts: Particle Size Effects

Stephen C. Parker
Carleton College

Charles T. Campbell
University of Washington

Recommended Citation

Parker, Stephen C., and Charles T. Campbell., "Reactivity and Sintering Kinetics of Au/TiO2(110) Model Catalysts: Particle Size Effects". *Topics In Catalysis*, vol. 44, no. 1-2, 2007. Available at: https://doi.org/10.1007/s11244-007-0274-z. . [Online]. Accessed via Faculty Work. Physics and Astronomy. *Carleton Digital Commons.* https://digitalcommons.carleton.edu/phys_faculty/2
The definitive version is available at https://doi.org/10.1007/s11244-007-0274-z

Reactivity and sintering kinetics of Au/TiO$_2$(110) model catalysts: particle size effects

Stephen C. Parker[a] and Charles T. Campbell[b,*]

[a]*Department of Physics and Astronomy, Carleton College, Northfield, MN 55057, USA*
[b]*Department of Chemistry, University of Washington, Seattle, WA 98195-1700, USA*

We review here our studies of the reactivity and sintering kinetics of model catalysts consisting of gold nanoparticles dispersed on TiO$_2$(110). First, the nucleation and growth of vapor-deposited gold on this surface was experimentally examined using x-ray photoelectron spectroscopy and low energy ion scattering. Gold initially grows as two-dimensional islands up to a critical coverage, θ_{cr}, after which 3D gold nanoparticles grow. The results at different temperatures are fitted well with a kinetic model, which includes various energetic parameters for Au adatom migration. Oxygen was dosed onto the resulting gold nanoparticles using a hot filament technique. The desorption energy of O$_a$ was examined using temperature programmed desorption (TPD). The O$_a$ is bonded $\sim$40% more strongly to smaller (thinner) Au islands. Gaseous CO reacts rapidly with this O$_a$ to make CO$_2$, probably via adsorbed CO. The reactivity of O$_a$ with CO increases with increasing particle size, as expected based on Brønsted relations. Propene adsorption leads to TPD peaks for three different molecularly adsorbed states on Au/TiO$_2$(110), corresponding to propene adsorbed on gold islands, to Ti sites on the substrate, and to the perimeter of gold islands, with adsorption energies of 40, 52 and 73 kJ/mol, respectively. Thermal sintering of the gold nanoparticles was explored using temperature-programmed low-energy ion scattering. These sintering rates for a range of Au loadings at temperatures from 200 to 700 K were well fitted by a theoretical model which takes into consideration the dramatic effect of particle size on metal chemical potential using a modified bond additivity model. When extrapolated to simulate isothermal sintering at 700 K for 1 year, the resulting particle size distribution becomes very narrow. These results question claims that the shape of particle size distributions reveal their sintering mechanisms. They also suggest why the growth of colloidal nanoparticles in liquid solutions can result in very narrow particle size distributions.

KEY WORDS: Catalysis; gold; TiO$_2$; sintering; nanoparticles; particle growth; selective oxidation.

1. Introduction

Gold nanoparticles supported on titania surfaces have been extensively studied for their applications as catalysts for low-temperature CO oxidation, selective propene oxidation, and other catalytic and photocatalytic oxidation reactions [1–9]. One very important conclusion that has arisen from these studies of gold catalysis has been that the size and/or thickness of the gold nanoparticles is of vital importance for the activity and selectivity of the catalyst. For instance, there is a notable size requirement for the gold particles in low temperature CO oxidation catalysts, which need to be $\leq$3 nm in diameter to be most active, and particles much bigger than 6 nm are almost inactive in this reaction. Experiments such as these have spawned a variety of questions about different aspects of gold catalysis that remain unanswered, such as why there is a "magic island size" on which certain reactions can take place, or why gold, a seemingly unreactive noble metal, should be active for so many catalytic reactions. The pursuit of trying to answer puzzling questions such as these has been the focus of many theoretical and experimental groups, and we are still striving to find many of the

answers. Much progress has been made in the past decade on this subject, however.

Much of the research done on these systems, including that in our own group, have addressed the reaction mechanism or the catalytically active sites using a single-crystal model catalyst approach. The model catalysts of most interest here employ well-defined oxide single crystals (or thin, ordered oxide films on metal single crystals) as the support material, onto which a transition metal is vapor deposited in some way [10–22]. Work in our group in this arena, for example, has focused on the vapor deposition of gold onto stoichiometric single-crystal TiO$_2$(110) surfaces [17–22]. Once the nanoparticles had been made on the surface, a variety of characterization spectroscopies and microscopies were then used to explore and characterize the resulting system.

One of the interesting hurdles that still faces the catalytic industry today is the task of trying to develop working catalysts that resist the long term effects of sintering. For catalysis by gold, this is a particularly acute problem, since the particles must remain extremely small to be active. Even though a perfect catalyst might be prepared with just exactly the right size and thickness of particles needed to produce the desired selectivity and reactivity, it might then rapidly sinter and thicken into particles that are much too big to be catalytically active. Theoretical modeling of the sintering process for catalysts,

to correctly extrapolate from short time-scale measurements to make long-term predictions has been hampered by a lack of an accurate kinetic description of the process. This means that a prospective catalyst that shows promise needs to be tested for time periods on the order of which they expect to be used in their application (which can be on the order of years). This is a major obstacle for the development of new catalysts.

These questions and hurdles provide a considerable number of opportunities for theorists and experimentalists to attempt to gain insight into the many conundrums that surround gold catalysis. Our group has focused on three specific areas of research regarding gold catalysis in an attempt to provide some perspective from a model-catalyst viewpoint. These three areas of experimental research, which we will review in this paper, are: (1) studies of particle growth kinetics during the vapor deposition of Au atoms onto a TiO$_2$(110) surface to make model catalysts consisting of Au nanoparticles supported on TiO$_2$(110), (2) studies of the chemical reactivity of the resulting model catalysts surfaces toward catalytically interesting molecules during adsorption and titration reactions of adsorbed catalytic intermediates, and (3) studies of the thermal stability of these Au nanoparticles on the TiO$_2$(110) surface and their sintering kinetics. In this study of sintering kinetics, we also developed a new method for probing sintering kinetics, temperature-programmed low-energy ion scattering (TP-LEIS), which is unique in that it allows a large range of apparent activation energies involved in long-term sintering to be conveniently probed in a single short-term experiment.

In order to extrapolate these measurements of short-term sintering kinetics to make predictions of the long-term sintering behavior of Au/TiO$_2$ catalysts, we developed a new kinetic model for sintering based on an atomistic mechanism (Ostwald ripening), which will also be reviewed here. Our results indicate that this new model is more accurate than previous atomistic models for sintering kinetics, and is the only model that fits experimental data over a wide temperature range using physically reasonable kinetic parameters [22]. This model predicts that, in the size range of interest in gold catalysis, long-term sintering leads to a strong focusing of the particle size distribution. This calls into question a classical method for determining sintering mechanisms based only upon the shape of the resulting particle size distributions. Our new model also offers an explanation for the particle-size focusing (decrease in the relative width of the particle size distribution) which is often observed during liquid-phase synthesis of colloidal nanoparticles.

2. Experiment

All of the experiments outlined in this work have been performed in a Leybold–Heraeus ultrahigh vacuum (UHV) system described in much more detail elsewhere [17,18]. Briefly, the system has two chambers with a base pressure of $\sim 2 \times 10^{-10}$ mbar with capabilities of x-ray photoelectron spectroscopy (XPS), low energy ion scattering (LEIS), low energy electron diffraction (LEED), and temperature programmed desorption (TPD). A polished TiO$_2$(110) crystal (Commercial Crystal Laboratories) is mounted on a Ta plate and can be resistively heated and cooled with liquid N$_2$, such that temperatures from ~ 150 to 1000 K can be obtained. Temperature is monitored by a chromel/alumel thermocouple glued directly to the crystal.

The stoichiometric TiO$_2$ (100) surface was prepared using standard preparation recipes [17,18]. Briefly, the surface is cleaned with a 1.0 keV argon ($\sim 2 \times 10^{-5}$ mbar) ion sputter and subsequently annealed in a partial pressure of O$_2$ ($\sim 3 \times 10^{-6}$ mbar) for 10 min at 873 K. The sample is then allowed to cool in the same partial pressure of O$_2$ to 373 K. This recipe results in a well ordered LEED pattern. The oxygen (as well as other gases used in experiments) could be dosed onto the surface using a directed doser, with the nozzle of the tube located very near the crystal.

Gold was deposited onto the surface using a resistively heated Ta boat that was coated with a high temperature ceramic glue to prevent the gold from wetting the boat and breaking the contacts [17]. XPS was used as a quantitative measure for how much gold had been deposited on the surface, while LEIS was used to quantitatively determine how much of the surface was covered by at least one atomic layer thick gold (or a so-called "Au area fraction"). The area fraction of the surface covered by gold could be monitored as a function of temperature during a linear ramp using temperature programmed low energy ion scattering (TP-LEIS) [22].

3. Results and discussion

3.1. Growth kinetics of Au nanoparticles on TiO$_2$(110)

First, we characterize the growth of vapor-deposited gold on a TiO$_2$(110) surface. Since gold-gold bonds are much more favorable than gold-oxide bonds, one might expect the growth mode to be a Volmer–Weber type, where three dimensional islands are formed from the onset of growth. We have found that this is not the case but instead, the initial growth is kinetically limited at room temperatures and below to just two dimensional islands. Only after a certain critical coverage of gold has been deposited onto the surface does the growth proceed into the third dimension [17].

By experimentally measuring both XPS and LEIS as small amounts of gold are deposited onto the substrate, we can obtain information about the resultant structure of the gold on the surface. Figure 1 shows the results of growth experiments that were performed at three different substrate temperatures (153 K, 213 K, and

293 K) [17]. The area fraction of the surface covered by at least one layer of Au (as measured by LEIS) is plotted on the vertical axis, while the total amount of Au that has been deposited onto the surface (as measured by XPS) is plotted on the horizontal axis. The units on each axis are monolayers (ML), where 1 ML is defined as the packing density of an Au(111) plane, 1.39×10^{15} atoms/cm², which is equivalent to an effective thickness of 2.35 Å at the density of bulk gold. Although a combination of XPS and LEIS do not give information about individual islands on the surface, these techniques combine to give information on a more global scale about the average thickness of the gold islands on the surface. We use this feature to our advantage, since the combination of these techniques allows us to sample large areas of the surface without needing to worry about the issues of proper sampling faced in microscopy.

As seen in figure 1, during the initial stages of growth at all three temperatures, the growth follows a straight line with a slope of 1.0. A slope of 1.0 on this graph corresponds to a layer by layer growth mode, since every
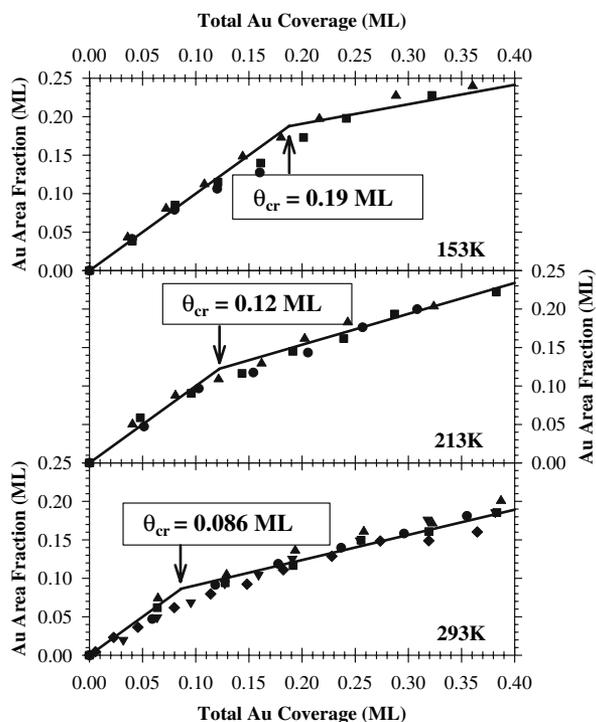

Figure 1. The area fraction of Au islands on TiO₂(110) as a function of total Au coverage for Au deposition at ∼0.3 ML/min at three different substrate temperatures: (a) 153 K, (b) 213 K, and (c) 293 K. Area fractions are determined from the integrated LEIS Au signal and the coverages are calculated from the vapor flux determined by XPS. The slope of the solid line in the low-coverage layer-by-layer region is 1, representing adatoms adding to the edges of two-dimensional islands with a probability of 1. The solid line fit beyond the layer-by-layer represents that an adatom landing on the surface has a fixed probability of ending up in the first layer. The intersection of these two lines is taken as the critical coverage (θ_{cr}). θ_{cr} is shown to increase with decreasing temperature. From [17].

deposited gold atom covers part of the TiO₂ substrate. As more and more Au is deposited, though, a transition from 2D growth to 3D growth is seen to occur and can be recognized by a change in the slope of the line. The critical point at which the growth changes from the 2D mode to the 3D mode is called the critical coverage (θ_{cr}). As can be further seen in figure 1, the critical coverage is found to be a function of the temperature of the substrate. The critical coverage ranges from 0.086 ML at 293 K to 0.19 ML at 153 K. Thus, as the temperature of the substrates decreases, the critical coverage is found to increase.

The dependence of the critical coverage on other experimental parameters was also explored. For instance, it was found when the Au deposition rate was varied over almost two orders of magnitude, the critical coverage was independent of the vapor flux and remained constant. Furthermore, when TiO₂ surfaces were specially prepared with extra defects (either by creating annealed-induced defects or sputter-induced defects), a higher critical coverage resulted as compared to a non-defected surface [17].

These experimental results were modeled using kinetic models discussed in depth elsewhere [17]. As gold is deposited onto the surface, the adatoms diffuse around on the substrate until they bump into other adatoms also diffusing on the surface. Once enough atoms come together to form a stable nucleus, this site becomes a nucleation point for an island on the surface (probably at a defect). We assume that the dimer is more stable than two monomers (critical nucleus size = one). The nucleation stage occurs quite rapidly at the onset of the growth, and a saturation number density of islands is quickly reached. Other gold adatoms diffusing on the surface are now much more likely to encounter an already nucleated island than another diffusing adatom, so the growth proceeds by addition of these diffusing adatom to the edges of the existing islands. Once the 2D islands have grown to a certain critical area, the growth of the island in the third dimension is allowed and as a consequence, the growth in the lateral dimension is greatly suppressed. This critical area occurs when two diffusing adatoms meet on the top of a gold island, and thereby nucleating a second layer island on top of this two dimensional island. Once this stable nucleus is present on top of the island, other adatoms that happen to be on top of the island (such as gold atoms that land on top of the island) are now much more likely to attach to this spot in the second layer instead of downstepping, and the growth in the third dimension begins.

This kinetic model can be used to predict a critical coverage as a function of the saturation number density of islands (N) on the surface and the critical island area (A_{cr}) [17]. Although neither of these quantities are directly measured using XPS or LEIS, their product is the critical coverage which we do measure ($\theta_{cr} = N * A_{cr}$) on our

surface. In this kinetic model [17], it was found that N and A_{cr} are given by:

$$N \propto \left(\frac{F}{D_o}\right)^{1/3} \quad \text{and} \quad A_{cr} = \left(\frac{p^2 D_1 a^2}{FN}\right)^{1/4}$$

where F is the incoming vapor flux of Au, D_o is the diffusion constant of the gold on the substrate, p is the probability of a gold atom "down-stepping" from the top of an island to the first layer, D_1 is the diffusion constant of gold adatoms on top of gold islands, and a is the lattice constant. The two diffusion constants and the probability of down-stepping have temperature dependences which are introduced in a Arrhenius-like way. When these two quantities are multiplied together, we proved that the critical coverage simplifies to [17]:

$$\theta_{cr} \propto \left(\frac{p^2 D_1 a^2}{D_o}\right)^{1/4}$$

This result predicts that the critical coverage we measure in our experiment should not depend on the flux but should vary with temperature, since p, D_1, and D_o all have associated temperature dependences. Furthermore, on surfaces with a number of defects present, the diffusion constant of gold on the substrate will be effectively reduced, since gold adatoms will get "trapped" at these defects for longer periods of time (due to the stronger bonding at these sites). This also fits our experimental data, since a smaller D_o will yield a higher θ_{cr}.

As can be seen, good qualitative agreement between kinetic modeling and experimental data was found. We also further explored the temperature dependence of the critical coverage by making an Arrhenius plot of the critical coverage vs. the inverse of the temperature. This resulted in a slope of 260 K ± 20 K, which corresponds to a negative apparent activation energy of −2.2 kJ/mol [17]. Depending on the role of defects on the substrate and the size of the barrier for downstepping at the edge of the island (the so-called "Schwoebel" barrier), this apparent activation energy relates the diffusion energies of gold on the islands to gold on the substrate. Defects play a crucial role in this analysis.

3.2. Chemical reactivity studies of Au/TiO₂(110)

As a result of the growth kinetics experiments outlined above, we can deposit various known amounts of gold onto the TiO₂ surface, such that the resulting particles are of well-defined thicknesses. Thus, the average particle thickness can be characterized by XPS and LEIS measurements of the grown islands once they have been deposited onto the substrate.

We used a hot filament technique [23,24] to help dissociate O₂ gas and deposit oxygen adatoms (O_a) on the gold islands [18,19], since dissociative adsorption of O₂ has not been found to occur on bulk gold [23]. Any

oxygen that does dissociatively adsorb on the surface even at high pressures of O₂ would be rapidly cleaned away by low level impurities in the chamber and hard to detect [19]. The dissociation of O₂ may be the rate-limiting step of catalytically interesting oxidation reactions such as CO oxidation on nano-Au.

After dosing O₂ at 2×10^{-5} mbar for 120 min using the hot filament technique, it was found that 35% of the gold island area was covered with O_a, regardless of the thickness of the gold [18, 19]. This could be verified by examining the attenuation of Au LEIS signal by these adsorbed oxygen adatoms. Control experiments showed that LEIS measurement resulted in little to no removal of the adsorbed oxygen adatoms. We define 1 ML of O_a coverage to be equal to the amount of oxygen needed to completely cover the gold LEIS signal for the gold islands on the substrate (which corresponds to $\sim 1.5 \times 10^{15}$ oxygen adatoms per cm²) [19].

Figure 2 shows TPD spectra from the associative desorption of O adatoms as O₂ gas from gold islands of varying average thicknesses [19]. Note that a higher fraction of the TiO₂ surface is covered by gold islands when their average island thickness is > 6 layers compared to islands of average thickness of 1.3 layers. This is why the TPD peaks are larger for the higher island thicknesses. This result is expected and is only an artifact of our surface preparation technique. What is more
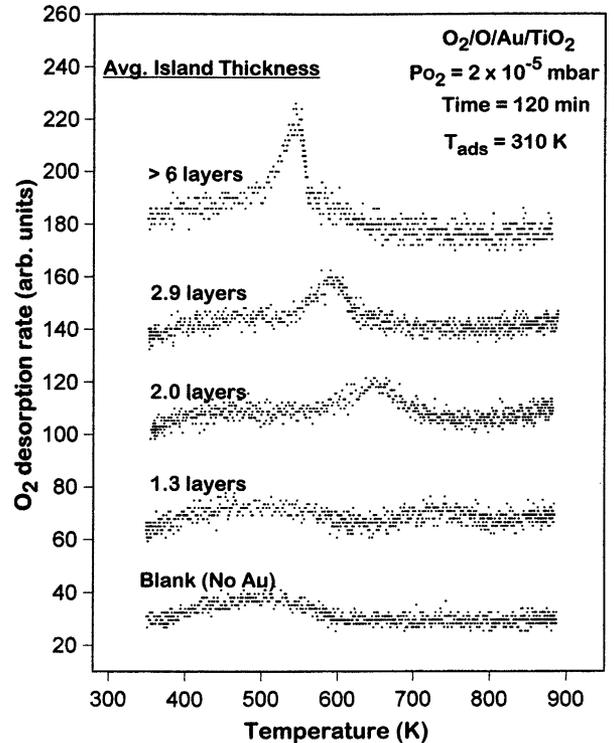

Figure 2. O₂ TPD curves for 0.35 ML of oxygen adatoms on Au islands of different average thicknesses in atomic layers. These islands covered the following fractions of the TiO₂(110) surface: 14% (1.3 layers), 28% (2.0 layers), 43% (2.9 layers), 60% (> 6 layers). From [19].

important to see on this figure is how the temperature of desorption changes due to the varying thicknesses of gold. At an average gold island thickness of 1.3 layers, O_2 desorbs at ∼740 K. When the gold islands are an average thickness > 6 layers, O_2 desorbs at 545 K. This is not due to changes in the initial local oxygen coverage on the Au islands, which was almost the same in all these TPD spectra (as proven by the attenuation of the Au LEIS signal by the oxygen adatoms) [19].

Since the desorption temperature of the O_2 from the thinner islands is ∼40% higher than that for the thicker islands, we conclude that the O_a is ∼40% more strongly bound to the thinner islands. From Brønsted relationships, a larger binding energy for oxygen adatoms indicates a lower activation energy for dissociative adsorption. This means that the thinner gold particles will be more active in dissociatively adsorbing O_2, which in turn could result in reactivity for oxidation catalysis.

We have also performed CO titration experiments on these surfaces with preadsorbed O_a [19]. Figure 3 shows titration curves, where the coverage of oxygen on the surface is measured as a function of time while a constant background of CO is introduced into the chamber. Experimental data is shown for two different thicknesses of gold islands. When thicker gold islands were grown on the surface, they behaved very nearly the same as the 2.2-layer islands, so higher coverage data is not shown. Also plotted on the graph are theoretical fits to the data,

assuming a first order-reaction rate in oxygen coverage. A first-order rate constant, k, is defined examining the time dependence of the oxygen coverage (θ_o). Specifically, fitting an equation of the form $d\theta_o/dt = -k\,\theta_o$ will yield the rate constant. As can be seen, the reaction rates are well fitted with this first-order model. The value for the rate constant for 1.2-layer islands was found to be $0.0010\ s^{-1}$ while for 2.2-layer islands it was $0.0023\ s^{-1}$, proving that O_a is less reactive on the smaller gold particles, where it is more strongly adsorbed. Thus the association reaction ($CO_a + O_a \rightarrow CO_{2,g}$) gets faster as the oxygen adsorption strength decreases, again as expected from Brønsted relations. Furthermore, we also varied the CO pressure in the chamber and measured the resulting rate constant. A plot of the $\ln k$ versus the $\ln P_{CO}$ yields a straight line with a slope of 1.1 +/− 0.1, which indicates that the production is first-order in CO pressure at these low CO pressures and moderate-to-high O_a coverages. Note that at these temperatures and CO pressures, the coverage of CO_a on the gold particles is expected to be first-order in CO pressure. Interestingly, the CO reaction order in quasi-steady-state CO oxidation catalysis at higher CO pressures was found to be much smaller (from 0.05 to 0.4) [25,26], which suggests that oxygen adsorption is the most rate-limiting step in the net catalytic reaction at those higher pressures (i.e., has the largest degree of rate control). Note that the rate *per CO collision with the surface* is much, much higher here in our experiments than it is at those more realistic catalytic reaction conditions. This lower rate per CO collision at higher CO pressures proves that the O_a coverage on the gold surfaces was much lower there.

Figure 3 also shows that any O_a that is present on the gold surface is rapidly titrated away even in this small CO partial pressure with a time constant of ∼10 min. This highlights the high reactivity of O_a on Au surfaces, which arises from the weak O-Au bonding. For islands of ∼2 atom thickness, the rate increases slowly with temperature, with an apparent activation energy of ∼11 kJ/mol, and shows a first-order rate in CO pressure and oxygen coverage, similar to bulk Au(110) [19].

To summarize, oxygen adatoms bond more strongly to smaller Au particles, which should decrease the barrier for dissociative O_2 adsorption. This stronger bonding of O adatoms to smaller particles makes them less reactive with CO, but that step is extremely fast and so is not the rate-determining step in real catalysis. If the rate-determining step is dissociative O_2 adsorption, then the smaller particles will be more catalytically active.

We have also examined the adsorption of propene ($CH_3CH=CH_2$) on the Au/TiO₂(110) surface, to produce possible adsorbed intermediates in selective propene oxidation over Au/TiO₂ [2]. When a clean TiO₂(110) surface at 120 K is exposed to propene doses of 0.001 L–0.01 L (uncorrected for the directed doser's enhancement factor), TPD showed that molecular
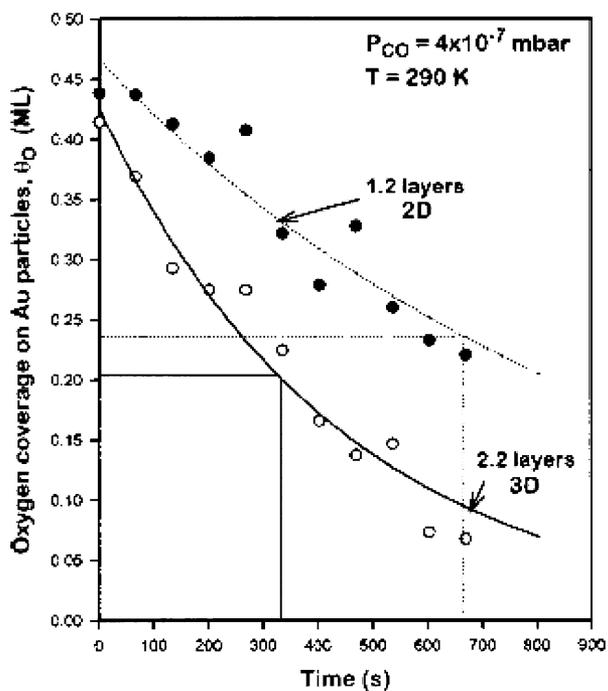

Figure 3. Titration curves of the oxygen coverage versus time upon exposure of oxygen adatoms preadsorbed on Au nanoparticles on TiO₂(110) to CO gas. The half-life of O_a on the ∼1 atom thick (2D) islands is approximately twice that on the 2-atom thick (3D) islands. From [19].

propene desorbs from the surface at temperatures of 188 K and 180 K, respectively [20]. Using a first-order Redhead analysis [27] and the heating rate of 5 K s^{-1}, the activation energy for propene desorption was calculated to be 47 kJ/mol in the limit of zero coverage, assuming a prefactor of 10^{13} s^{-1} [20]. More recent results show that the prefactor for propene desorption should be $\sim 10^{15}$ s^{-1} instead [28,29], which would increase this activation energy to 52 kJ/mol. This is a more accurate estimate. The slope versus coverage was found to be -2.8 (kJ/mol)/ML [20], due to repulsive interactions between propene molecules on the surface.

As gold is deposited onto the surface, two new desorption peaks become apparent after dosing propene onto the surface [20]. Figure 4 shows a typical TPD resulting from a surface that is 16% covered by 1.5 ML thick gold islands after varying doses of propene (from 0.001 L to 0.01 L). The peak due to propene adsorbed molecularly on 5-fold coordinate Ti sites of the TiO₂ surface, mentioned above, desorbs in a peak from 155 K to 210 K. The two additional peaks not seen on a clean TiO₂ surface are a low temperature peak from 125 K to 155 K and a high temperature peak at 210 K–295 K. Based on LEIS results, these were attributed to propene molecularly adsorbed on the top of Au islands and on the edges of Au islands (also bonded to Ti sites), respectively [20]. The adsorption energies for propene were estimated to be 40 and 73 kJ/mol, respectively, using the mean TPD peak temperatures as above. Note, however, that the 210 K–295 K peak shifted to higher temperature with decreasing Au particle size, indicating that smaller particles bind propene more strongly at

their edges [20]. Furthermore, it was seen that at the lowest propene coverages, the desorption peak for propene on pure TiO₂ sites was not populated, which proves that adsorbed propene is mobile at these temperatures and moves to the more stable adsorption sites at the edges of the gold islands [20].

3.3. Sintering kinetics and applications to Au/TiO₂(110)

Sintering is a major mode of deactivation for many catalysts, especially for late transition metal particles dispersed on oxides or other supports. These catalysts sinter or ripen with time on-stream, starting from a collection of many small, highly dispersed particles and eventually converting to their thermodynamically-preferred state: fewer, larger particles [30–33]. The thermal stability of Au nanoparticles on TiO₂(110) has been the subject of considerable study, mainly by STM [33–40], because of the importance of this system as a model catalyst and because sintering is a real impediment to the industrial application of Au/TiO₂ catalysts. It was concluded that sintering occurs mainly by the Ostwald ripening mechanism [33–35], although particle diffusion/coalescence also occurs, and may even dominate in some conditions [34, 36–38]. In catalyst systems like this where the metal-area-normalized activity decreases strongly with particle size in the 3–6 nm range, sintering leads to even more dramatic deactivation than in more typical systems where the area-normalized activity remains nearly constant.

Currently there is no reliable way of predicting the sintering kinetics, so any newly developed catalyst must be tested for the total duration of its required lifetime, often on the order of one year. Development of new catalyst materials could be accelerated dramatically if there were a kinetic model, which could accurately predict long-term sintering based on short-term kinetic measurements.

We recently derived an improved kinetic model for sintering of supported metal nanoparticles [22]. It follows the pioneering model of Wynblatt and Gjostein (WG) [30], but removes two assumptions that create dramatic errors in sintering rates for particles smaller than 6 nm in diameter, including: (1) use of the Gibbs–Thomson (GT) relation assuming that the surface free energy of metal particles is independent of size, and (2) neglect of all but the first-order terms in a Taylor series expansion. Recent microcalorimetry measurements have shown these assumptions to be untrue in that metal particles smaller than 6 nm have much higher surface free energies than large particles. A modified bond-additivity (MBA) model more accurately estimates particle energy versus size [21]. This estimate was incorporated into our new kinetic model [22]. We review below results which show that this model can accurately reproduce the measured short-term sintering kinetics of Au particles on
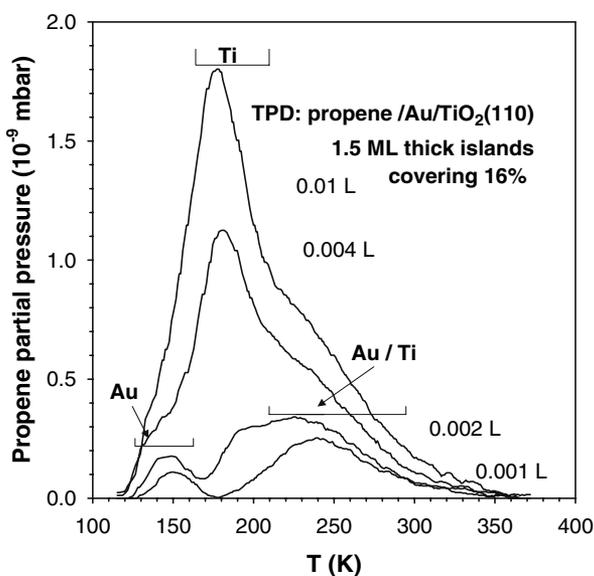

Figure 4. TPD spectra, at 5 K/s, of propene adsorbed on TiO₂(110) with Au islands of average thickness 1.5 atomic layers covering ~16% of the surface at 120 K. "Au": peaks at 125–155 K, due to propene adsorption on the tops of gold islands. "Ti": peaks at 155–210 K, due to adsorption on the TiO₂(110). "Au/Ti": peaks at 210–295 K, due to propene adsorbed at the edges of gold islands. From [20].

TiO$_2$(110) at different loadings, and use this model to predict sintering after long times (1 year) [22]. This long-time behavior shows the dramatic effects of this improvement in the kinetic model upon both the resulting average particle size and their size distribution.

By combining a linear temperature ramp with simultaneous measurement of the LEIS peaks (TP-LEIS), we have examined the kinetics of sintering over short (~5 min) time periods but in way that conveniently samples a large range of activation energies, in an attempt to learn more about long term sintering under isothermal conditions [22]. Figure 5 shows TP-LEIS experimental data for thermal sintering of Au on TiO$_2$(110) for three different initial coverages of gold. As can be seen, the area fraction of the surface covered by gold slowly decreases for all three loadings as the particles sinter and uncover the TiO$_2$ surface. Furthermore, the sintering is seen to occur with a similar apparent rate over this full, very broad range of temperatures. We performed control experiments wherein Au/TiO$_2$(110) was exposed to the same ion beam flux for the total time as used in these TP-LEIS experiments, but without heating. The negligible loss of Au LEIS signal proved that its removal by sputtering is much slower than by sintering.

Standard rate-equation methods of modeling this behavior do a very poor job reproducing this extremely broad temperature dependence. The solid lines in figure 5, though, are the results of a theoretical model outlined below, which includes a different model for particle energetics for nanometer sized particles based on measurements from single crystal microcalorimetry done in our group [21]. These energetics are quite different from the energetics that standard models in the past have used for kinetic predictions, and we find that they can be used to fit our data rather well [22].

Microcalorimetry measurements from Pb on MgO(100) [21] have shown that the surface free energy of small particles increases much more dramatically with decreasing size than predicted by a Gibbs–Thomson (GT) relation. The GT relation states that the chemical potential of a metal atom in a particle of radius R, $\mu(R)$, differs from that of an atom in the bulk, $\mu(\infty)$, by

$$\mu(R) - \mu(\infty) = \frac{2\gamma\Omega}{R}$$

where γ is the surface free energy of the metal and Ω is the atomic volume of the metal. By using a modified pairwise bond additivity (MBA) model, we could better reproduce the dramatically different energetics seen in the calorimetry experiments for the catalytically interesting nanometer-scale sized fcc metal particles [21]. Previous atomistic models of sintering kinetics, such as the work by Wynblatt and Gjostein [30], used the GT relation in their work.

Our new model is a modification of the Wynblatt/Gjostein model based on the "Ostwald ripening"
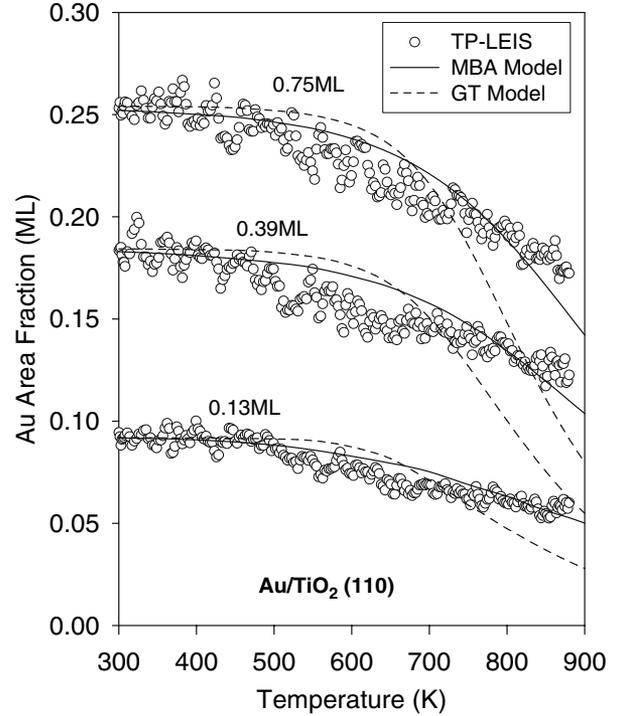

Figure 5. A comparison of experimental TP-LEIS data (at 1 K/s) for Au particles on TiO₂(110) with the MBA and GT Ostwald ripening kinetic simulations. The Au coverages are in units of ML, where 1 ML is defined as the Au(111) packing density, 1.39×10^{15} atoms/cm². The best-fit parameters were, from the bottom curve up:
0.13 ML: initial $<R>$ = 0.45 nm, FWHM = 0.20 nm, v_p = 4× 10^{12}sec⁻¹, E_{tot} = 327 kJ/mol (MBA) and 240 kJ/mol (GT).
0.39ML: $<R>$ = 0.64 nm, FWHM = 0.60 nm, v_p = 4×10¹²sec⁻¹, E_{tot} = 287 kJ/mol (MBA) and 220 kJ/mol (GT).
0.75ML: $<R>$ = 0.75 nm, FWHM = 1.15 nm, v_p = 4×10¹²sec⁻¹, E_{tot} = 263 kJ/mol (MBA) and 210 kJ/mol (GT). From [22].

mechanism [30]. Ostwald ripening is a process whereby the larger islands grow larger while the smaller islands grow smaller, due to the movement of individual atoms that leave one island and then join another. Since the larger islands are more stable due to the stronger bonding of the atom to those islands, there will be a gradual increase of the average island size on the surface. Specifically, we modified the "interface-controlled" limit of the Wynblatt-Gjostein model [30], in which the rate of change of a radius of a particle on the surface is rate limited by the attachment/detachment process at the edge of the island. In the original Wynblatt–Gjostein model, the authors took a Taylor series expansion of exp[$-2\gamma\Omega/(RkT)$] in calculating this rate of change, and kept only the first term of the expansion [30]. We have found that this creates dramatic errors in the sintering rates for particles of nanoscale sizes. Without using this truncated Taylor expansion, the rate of change of the radius of a particle is given by:

$$\frac{dR}{dt} = \frac{K}{R}\left(\exp\left[\frac{-E_{tot}}{kT}\right]\right)\left(\exp\left[\frac{E(R^*)}{kT}\right] - \exp\left[\frac{E(R)}{kT}\right]\right)$$

where k is Boltzmann's constant and T is the temperature. The other variables in this equation are described in more detail below.

Here, $E(R)$ (and $E(R^*)$) are the chemical potential difference between an atom in a particle of radius R (or R^*) and that of an atom in a particle of infinite radius. R^* is the inverse of the average of $1/R$ for all the particles. R^* can be thought of as the dividing line between whether or not an island will tend to grow larger or begin to sinter away. Furthermore, once the smaller islands on the surface have sintered away, R^* will slowly become larger, therefore allowing the sintering process to continue, since a new set of islands will now exist below this threshold. It is these $E(R)$ values that are obtained using the MBA model that are very different from the $E(R)$ values from a GT model. E_{tot} is a collection of energetic parameters for the gold on the surface, such that $E_{tot} = \Delta H_{sub} - E_{ad}^s + H_m^s$. These energies are the bulk sublimation energy, the adsorption energy of a monomer on the support, and the activation energy for diffusion of a monomer on the support, respectively. K is a constant which depends on the contact angle of the particle on the surface (θ), the prefactor for diffusion along the edge of the particle (v_p), the metal's lattice constant (a), and the solid metal's volume per atom (Ω), such that:

$$K = \frac{2v_p \Omega \sin\theta}{a(2 - 3\cos\theta + \cos^3\theta)}$$

.

By scaling the energies by the metal-metal bond strength and scaling their effective radii by $\Omega^{1/3}$, we can extrapolate our MBA energetics from Pb/MgO to other fcc metals for which calorimetric data does not exist [22]. In this way, we calculate what we expect to be a more accurate representation for $E(R)$ for these nanoscale particles, such that we can now accurately model the sintering of the Au/TiO$_2$ system.

We have used the MBA energetics for Au/TiO$_2$ to reproduce the large temperature range of sintering seen in TP-LEIS experiments [22]. A program which propagates an initial Gaussian distribution of islands using finite time differences methods was written to compare with the experimental data. To simulate a TP-LEIS experiment, the temperature was increased by an amount $B\Delta t$ in each time step Δt, where B is the heating rate (1 K/sec) for the experimental data. For other details, see [22]. The results of these simulations are the solid lines in figure 5. Simulations based on GT energetics could not be made to fit the experimental data over the broad temperature range of sintering anywhere near this well. As noted elsewhere [22], to perform these simulations we used a smaller average size and narrower size distribution for the starting Au particles than implied by STM observations. This is because we thought the STM experiments might have missed many of the smallest particles or they might

have sintered in the period required to stabilize the STM image. (Completing an STM image is inherently much slower than starting a TP-LEIS ramp.). Also, this was required to get this good fit to the TP-LEIS sintering data. Different defect types or groups of defects also probably stabilized differently the particles in the experiments, which broadens the size distribution but was not included in our model.

A very important implication of our model is that isothermal experiments like STM cannot easily monitor sintering kinetics of small nanoparticles because sintering finishes so rapidly after establishing a new temperature. This is because the effective activation energy changes so rapidly with the extent of sintering. This is consistent with many experimental observations that led us to propose this model [10], and the reason that we developed TP-LEIS to study sintering kinetics instead of doing normal isothermal kinetics experiments.

Note that the GT model under-predicts sintering rates compared to the better MBA model, but only if one uses the *same* parameters in both models. If one instead varies their parameters independently to fit the short-term sintering kinetic data as we did here in fitting the TP-LEIS data of figure 5 (which required using a smaller combined activation energy, E_{tot}, in the GT model), one then sees that the GT model over-predicts the sintering rates at longer times (higher temperatures in TP-LEIS). This problem with the GT model is also apparent in extrapolating isothermal sintering data to longer long times, as we will show below.

The importance of an accurate representation of small-particle energetics is highlighted by the long-term simulations seen in figure 6. Here, the temperature of the surface is not increased as in the TP-LEIS simulations; rather, the temperature is held constant and the distributions are allowed to evolve in time for periods up to a year, as in real catalytic applications. In the left panel of figure 6, the size distributions of islands are simulated using the energetics of GT model, whereas in the right panel the MBA energetics are used. The long-term sintering of gold particles turns out to give drastically different results in these two situations. After 1 year, it is seen that the average particle size is only ~1.5 nm in the MBA model, whereas they are over ~4.5 nm in the GT model [22]. This major difference in the two models underlines the importance of accurately representing the surface free energy of the gold atoms. Using the GT model, one would conclude that the gold particles would be inactive after one year's time, whereas with the MBA model, one would conclude that the gold particles would still be very reactive. We know of no long-term sintering data of such model systems against which to compare these predictions. Importantly, the presence of gases like O$_2$, which are absent here, are known to accelerate sintering rates [30–32], probably by changing the barriers for monomer migration steps when bonded to the migrating metal atoms.
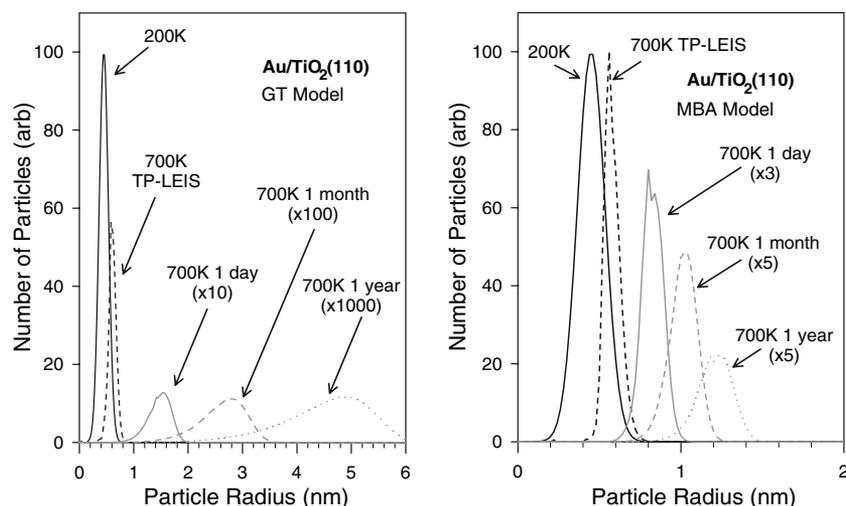
Figure 6. Predictions by the GT model (left) and MBA model (right) of the Au particle size distributions for 0.13 ML of Au on TiO₂(110) after sintering at 700 K for different times up to 1 year. The parameters in both models were determined by fitting to the same experimental temperature-programmed low-energy ion scattering (TP-LEIS) measurements of the initial sintering while the as-deposited Au particles were heated from 200 K to 700 K at 1K/s (see Fig. 5). From [22].

The particle size distributions in figure 6 show that the initial Gaussian distribution broadens with time and becomes asymmetric, with greater width on the lower-radius side of the maximum in both models. The width of the distribution is predicted with the MBA model to broaden much less compared to the GT model, for the same extent of sintering (i.e., for different times that result in the same final average radii).

These size distributions show that there are serious problems with the widely-used classical method for determining the sintering mechanism based solely upon the shape of the sintered particle size distribution. Basically, that method claims that the distribution is log-normal (i.e., has a sharp leading edge and a long tail to larger sizes) if the sintering occurs by particle diffusion / coalescence whereas it has a long tail to small sizes and a sharp trailing edge when sintering occurs by Ostwald ripening [41–43]. Clearly this is not true when one includes the proper kinetic rate laws and particle-size-dependent energetics. The derivation of the log-normal distribution assumes that the probability that two particles agglomerate is independent of their size [41,42]. This is certainly not the case, since their diffusion constant has a very strong particle-size dependence (see below). We conclude that, in the size range below ∼8 nm in diameter, one cannot use the shape of the particle size distribution to determine sintering mechanisms. A recent study of sintering mechanisms and particle size distributions using electron microscopy by Datye et al. [44] led to a similar conclusion.

Interestingly, the results of figure 6 also have important implications with respect to the size evolution of nanoparticles during the liquid-phase synthesis of colloidal nanoparticles. Talapin, Rogach et al. [45–46] developed a model based on Ostwald ripening

kinetics and the Gibbs–Thomson relation which they used to calculate the size evolution of nanoparticles during synthesis under reaction, diffusion, and mixed reaction-diffusion rate control. They performed Monte Carlo simulations of Ostwald ripening of an ensemble of growing nanoparticles in liquid solutions. They found conditions which lead to "focusing" of the particle size distribution under mixed diffusion-reaction control [45,46]. This is similar to the narrow size distributions that evolved in figure 6. They pointed out that this size focusing is only strong when one does not truncate the Taylor series expansion of $\exp[-2\gamma\Omega/(RkT)]$ as did Wynblatt and Gjostein [47] (see above). This truncation is also done in the classical theories of reaction-controlled growth of colloids such as Lifshitz–Slyozov–Wagner theory [45,46]. It is very important to realize that, while removing this truncation approximation does lead to more focusing in the size distribution, an even more dramatic size-focusing occurs when errors in the size-dependent chemical potential inherent to the GT model are repaired using the MBA model for nanoparticle energetics.

The treatment of sintering kinetics by WG [30, 47, 48] covered a number of other kinetic limits of the Ostwald-ripening mechanism beyond the "interface-controlled" limit discussed above. Since the factor $e^{\{\mu(R)-\mu(\infty)\}/kT}$ also appears in those rate expressions, it is also very important to include in them a proper treatment of the dramatic particle size effect on $\mu(R)$ mentioned above. This could be included in an approximate way using the MBA model described above, and should provide a dramatic improvement for particles smaller than 6 nm in diameter.

It is equally important to properly treat this dramatic particle size effect on metal atom energy in kinetic

models for sintering mechanisms dominated by particle diffusion/agglomeration instead of Ostwald ripening. This is because the factor $e^{\{\mu(R)-\mu(\infty)\}/kT}$ also appears directly in the rate expression for sintering by that mechanism, at least when the particle diffusion mechanism requires monomer diffusion around the perimeter of the particle [49,50]. This arises from the particle-size dependence of the rate constant for particle diffusion across the support, which has been written as:

$$D(R) = \frac{3\Omega^2}{\pi R^4} Dc_\infty \exp\left[\frac{\mu(R)-\mu(\infty)}{kT}\right],$$

where D is a constant. It is clear from figure 3 that one cannot neglect the particle size effect in the surface energy (i.e., assume the surface energy is a constant) when calculating $\mu(R)$ in this equation. Since this size effect is huge (see above) and enters in the resulting kinetic equations in an Arrhenius-like form (i.e., exponentially), it is a very serious error for small particle sizes. Again, using the MBA model should provide a much better approximation and should improve substantially any kinetic model based on this type of equation.

4. Conclusions

Gold clusters can be prepared on TiO$_2$(110) that are mainly 2D or 3D. Their reactivity depends on thickness (size). The bonding of O$_a$ is ~40% stronger to Au clusters that are only one atom thick compared to large Au particles. This O$_a$ is very reactive in CO titration experiments, but less reactive when more strongly bonded to the Au (i.e., on smaller particles). Three different molecular adsorption states were found for propene on Au/TiO$_2$(110) by TPD: on the tops of gold islands, at Ti sites on the edges of Au islands, and on Ti sites in Au-free areas on the titania. The sintering of gold particles on the TiO$_2$(110) surface were both experimentally measured using TP-LEIS and theoretically modeled using a modified bond additivity model in conjunction with an Ostwald ripening model developed by Wynblatt and Gjostein. The MBA model was necessary to more accurately represent the energetics of nanometer sized particles, as probed by single crystal adsorption microcalorimetry. This predicts dramatically narrower particle size distribution after long-term sintering compared to standard theories, which also suggests an explanation for size focusing observed during liquid-phase synthesis of colloidal nanoparticles.

Acknowledgments

References

[1] M. Haruta, Catal. Today 36 (1997) 153.
[2] T. Hayashi, K. Tanaka and M. Haruta, J. Catal. 178 (1998) 566.
[3] M. Haruta, Cattech 6 (2002) 102.
[4] M. Valden, X. Lai and D.W. Goodman, Science 281 (1998) 1647.
[5] M. Valden, S. Pak, X. Lai and D.W. Goodman, Catal. Lett. 56 (1998) 7.
[6] M.S. Chen and D.W. Goodman, Science 300 (2004) 252.
[7] D.W. Goodman, Catal. Lett. 99 (2005) 1.
[8] S.S. Lee, C.Y. Fan, T.P. Wu and S.L. Anderson, J. Am. Chem. Soc. 126 (2004) 5682.
[9] S. Lee, C.Y. Fan, T.P. Wu and S.L. Anderson, Surface Sci. 578 (2005) 5.
[10] C.T. Campbell, Surface Sci. Reports 227 (1997) 1.
[11] C.T. Campbell, A.W. Grant, D.E. Starr, S.C. Parker and V.E. Bondzie, Topics Catal. 14 (2000) 43.
[12] H.J. Freund, M. Baumer and H. Kuhlenbeck, Adv. Catal. 45 (2000) 333.
[13] C.R. Henry, Surface Sci. Reports 31 (1998) 231.
[14] A. Sanchez, S. Abbet, U. Heiz, W.D. Schneider, H. Hakkinen, R.N. Barnett and U. Landman, J. Phys. Chem. A 103 (1999) 9573.
[15] U. Heiz, F. Vanolli, A. Sanchez and W.D. Schneider, J. Am. Chem. Soc. 120 (1998) 9668.
[16] U. Heiz and E.L. Bullock, J. Mat. Chem. 14 (2004) 564.
[17] S.C. Parker, A.W. Grant, V.A. Bondzie and C.T. Campbell, Surface Sci. 441 (1999) 10.
[18] V. Bondzie, S.C. Parker and C.T. Campbell, J. Vac. Sci. Technol. A17 (1999) 1717.
[19] V. Bondzie, S.C. Parker and C.T. Campbell, Catal Lett. 63 (1999) 143.
[20] H.M. Ajo, V.A. Bondzie and C.T. Campbell, Catal. Lett. 78 (2002) 359.
[21] C.T. Campbell, S.C. Parker and D.E Starr, Science 298 (2002) 811.
[22] S.C. Parker and C.T. Campbell, Phys. Rev. B. 75 (2007) 035430.
[23] A. Sault, R.J. Madix and C.T. Campbell, Surf. Sci. 169 (1986) 347.
[24] N.D.S. Canning, D. Outka and R.J. Madix, Surface Sci. 141 (1984) 240.
[25] M.A. Bollinger and M.A. Vannice, Appl. Catal. B-Environ. 8 (1996) 417.
[26] M. Haruta, S. Tsubota, T. Kobayashi, H. Kageyama, M.J. Genet and B. Delmon, J. Catal. 144 (1993) 175.
[27] P.A. Redhead, Vacuum 12 (1962) 203.
[28] S.L. Tait, Z. Dohnálek, C.T. Campbell and B.D. Kay, J. Chem. Phys. 122 (2005) 164708.
[29] S.L. Tait, Z. Dohnálek, C.T. Campbell and B.D. Kay, J. Chem. Phys. 125 (2006) 234308.
[30] P. Wynblatt and N.A. Gjostein, in: Progress in Solid State Chemistry, Vol. 9, eds. J.O. McCaldin and G. A. Somorjai (Elsevier Science, Amsterdam 1975) p. 21.
[31] G.B. McVicker, R.L. Garten and R.T. Baker, J. Catal. 54 (1978) 129.
[32] G.A. Fuentes and E.-R. Salinas, in: Catalyst Deactivation, eds. C.H. Bartholomew and G.A. Fuentes (Elsevier Science, 1997), p. 573.
[33] X. Lai and D.W. Goodman, J. Mol. Catal. A 162 (2000) 33.
[34] C.E.J. Mitchell, A. Howard, M. Carney and R.G. Egdell, Surface Sci. 490 (2001) 196.
[35] A. Kolmakov and D.W. Goodman, Catalysis Lett. 70 (2000) 93.
[36] S. Kielbassa, M. Kinne and R.J. Behm, J. Phys. Chem. B 108 (2004) 19184.
[37] E.C.H. Sykes, F.J. Williams, M.S. Tikhov and R.M. Lambert, J. Phys. Chem. B 106 (2002) 5390.
[38] A. Kolmakov and D.W. Goodman, Chem. Record 2 (2002) 446.
[39] T. Okazawa, M. Fujiwara, T. Nishimura, T. Akita, M. Kohyama and Y. Kido, Surface Sci. 600 (2006) 1331.

[40] Y. Maeda, T. Fujitani, S. Tsubota and M. Haruta, Surface Sci. 562 (2004) 1.

[41] C.G. Granqvist and R.A. Buhrman, Appl. Phys. Lett. 27 (1975) 693.

[42] C.G. Granqvist and R.A. Buhrman, J. Catal. 42 (1976) 477.

[43] J. Sehested, A. Carlsson, T.V.W. Janssens, P.L. Hansen and A.K. Datye, J. Catal. 197 (2001) 200.

[44] A.K. Datye, Q. Xu, K.C. Kharas and J. M. McCarty, Catal. Today 111 (2006) 59.

[45] D.V. Talapin, A.L. Rogach, M. Haase and H. Weller, J. Phys. Chem. B 105 (2001) 12278.

[46] A.L. Rogach, D.V. Talapin, E.V. Shevchenko, A. Kornowski, M. Haase and H. Weller, Adv. Functional Mat. 12 (2002) 653.

[47] P. Wynblatt, R.A.D. Betta, N.A. Gjostein (1975), in: *The Physical Basis for Heterogeneous Catalysis*, eds. E. Drauglis and R.I. Jaffee (Plenum Press, New York), p. 501.

[48] P. Wynblatt and N.A. Gjostein, Acta Metallurgica 24 (1976) 1165.

[49] M.J. Jak, C. Konstapel, A.v Kreuningen, J. Crost, J. Verhoeven and J.W. Frenken, Surface Sci. 474 (2001) 28.

[50] M.J. Jak, C. Konstapel, A.v Kreuningen, J. Verhoeven and J.W. Frenken, Surface Sci. 457 (2000) 259.